

Radiation-induced segregation in Ni-Cu alloys

W. Wagner

Materials Science Division, Argonne National Laboratory, Argonne, Illinois 60439
and Hahn-Meitner-Institut für Kernforschung Berlin GmbH, Glienickerstrasse 100,
D-1000 Berlin 39, Germany

L. E. Rehn and H. Wiedersich

Materials Science Division, Argonne National Laboratory, Argonne, Illinois 60439

V. Naundorf

Hahn-Meitner Institut für Kernforschung Berlin GmbH, Glienickerstrasse 100,
D-1000 Berlin 39, Germany

(Received 18 March 1983; revised manuscript received 4 August 1983)

A detailed and systematic experimental study of the temperature and dose dependence of radiation-induced segregation in two alloys, Ni-10 at. % Cu and Ni-60 at. % Cu is presented. Auger-electron spectroscopy with ion sputtering was used to measure concentration-versus-depth profiles of irradiated and unirradiated specimens. The quantitative results are compared with a theoretical model, and "best-fit" defect solute parameters are obtained. In the 10-at. % Cu alloy, the model requires both preferential transport of nickel atoms toward the surface via the interstitial flux and preferential transport of copper atoms into the bulk via the vacancy flux to reproduce the observed concentration profiles. In the 60-at. % Cu alloy, the model explains the results equally well with preferential transport of nickel atoms by interstitials, preferential transport of copper atoms via vacancies, or a combination of these two transport mechanisms.

I. INTRODUCTION

Considerable experimental evidence has been found for nonequilibrium solute redistribution in alloys during irradiation at elevated temperatures.¹⁻⁴ As a result of this radiation-induced segregation (RIS), large changes in local composition have been observed in a wide variety of alloy systems. Theoretical models have been developed to describe RIS,⁵⁻⁸ which occurs because of preferential coupling between defect fluxes and fluxes of certain alloying elements. Mobile defects produced by the irradiation are reincorporated into the crystal structure at defect sinks, e.g., surfaces, dislocations, and grain boundaries. This spatially nonuniform defect annihilation induces defect fluxes toward the sinks. Any preferential coupling of alloying components to the defect fluxes will cause nonequilibrium redistribution in the alloy, i.e., enrichment or depletion of alloying elements in regions which experience a net influx or outflow of defects.

Besides the technical importance of RIS for materials applications in irradiation environments, a fundamental interest in the phenomenon results because the observed solute redistribution is a direct manifestation of interactions between individual solute atoms and point defects. Quantitative studies of RIS therefore offer a unique opportunity for determining properties of point defects in concentrated alloys.

The Ni-Cu system appears particularly well suited for fundamental investigations. As reported previously,^{9,10} strong segregation of nickel to external surfaces occurs

during irradiation of Ni-Cu alloys at temperatures between 420 and 610°C. This RIS has been studied by Auger depth profiling after irradiation with Ar⁺ or Ni⁺ ions, and by *in situ* Rutherford backscattering measurements during He⁺-ion bombardment. The Ni-Cu system has a strikingly simple phase diagram, exhibiting a continuous series of solid solution alloys at temperatures above 300°C. Therefore, RIS investigations and the application of theoretical models are not additionally complicated by phase transitions, which would require information on the physical parameters of all phases involved. Another reason that Ni-Cu is well suited for basic RIS studies is that it is one of the very few systems in which radiation effects and defect properties have been investigated in pure elements, in dilute alloys, and also in concentrated alloys.¹¹⁻¹⁴

In this paper, a detailed and systematic experimental study of the temperature and dose dependence of RIS in two alloys, Ni-10 at. % Cu and Ni-60 at. % Cu, is presented. Auger-electron spectroscopy (AES) with low-energy ion sputtering was used to obtain concentration profiles as a function of depth from the irradiated surfaces of the specimens. For quantitative evaluation of the data, theoretical calculations of RIS were performed for the corresponding experimental conditions with a certain set of defect parameters. The calculations are based on the model of Wiedersich *et al.*,⁶ which is summarized in Sec. II. Section III explains the experimental procedures, and the experimental results are presented in Sec. IV. The computational formalism used to obtain numerical solu-

tions of the equations describing the segregation process is outlined in Sec. V, which also gives the results which fit the experimental data. The main part of the discussion (Sec. VI) is a critical evaluation of the defect parameters.

II. THE THEORETICAL CONCEPT

This section summarizes the model of radiation-induced segregation in concentrated alloys recently presented by Wiedersich, Okamoto, and Lam,⁶ which allows preferential migration of vacancies and interstitials via A atoms or B atoms in a binary A - B alloy. Similarly, atom fluxes are partitioned into those occurring via vacancies and via interstitials. This approach permits the defect fluxes and atom fluxes to be expressed in terms of partial diffusion coefficients. As an example, the partial diffusion coefficient of A atoms via vacancies, D_A^v , can be written as

$$D_A^v = d_{Av} C_v, \quad (1)$$

where C_v is the atomic fraction of vacancies. The diffusivity coefficient, d_{Av} , of A atoms via vacancies contains all the geometric and kinetic information of the diffusion. For the face-centered-cubic structure of Ni-Cu, it can be written as

$$d_{Av} = a_0^2 \nu_{Av}, \quad (2)$$

where a_0 is the lattice constant and ν_{Av} represents the jump frequency with which an A atom exchanges with a vacancy on a neighboring site. If a preferential association between vacancies and A atoms (or B atoms) exists, such a factor will be incorporated into the exchange frequency, making it an "effective" jump frequency.

In their simplest form, the jump frequencies can be written as products of an "effective" preexponential frequency factor, ν_{Av}^0 , and a Boltzmann factor which contains the "effective" migration enthalpy, H_{Av} , i.e.,

$$\nu_{Av} = \nu_{Av}^0 \exp(-H_{Av}/kT), \quad (3)$$

where k is the Boltzmann constant, and T the absolute temperature.

Correspondingly, the partial diffusion coefficient for vacancies via A atoms is

$$D_v^A = d_{Av} C_A. \quad (4)$$

The partial diffusion coefficients for B atoms via vacancies and vacancies via B atoms are, respectively,

$$D_B^v = d_{Bv} C_v \quad (5)$$

and

$$D_v^B = d_{Bv} C_B, \quad (6)$$

with

$$d_{Bv} = a_0^2 \nu_{Bv}, \quad (7)$$

where ν_{Bv} is the effective exchange-jump frequency of a B atom-vacancy pair.

The partial diffusion coefficients of the elements via interstitials, and of interstitials via A and B atoms, are easily derived and are analogous to the quantities given for va-

cancies in Eqs. (1) to (7) with the subscripts and superscripts v replaced by i . However, the expressions for d_{Ai} and d_{Bi} will depend on the details of the interstitial migration mechanism. Since the details of interstitial migration in alloys are not well understood, we will assume that interstitials migrate via A atoms and/or B atoms, and that the partial diffusion coefficients can be written in the same form as those for vacancies. Thus

$$D_A^i = d_{Ai} C_i, \quad (8)$$

with

$$d_{Ai} = a_0^2 \nu_{Ai}. \quad (9)$$

Correspondingly,

$$D_i^A = d_{Ai} C_A, \quad (10)$$

$$D_B^i = d_{Bi} C_i, \quad (11)$$

and

$$D_i^B = d_{Bi} C_B. \quad (12)$$

The advantage of writing the partial diffusion coefficients in the form $D = dC$ is that the major compositional and, therefore, spatial dependence resides in the factor C , whereas d contains the diffusional information for the atom-vacancy or atom-interstitial complexes. In particular we note that the two quantities d_{Av} and d_{Bv} can be obtained from tracer-diffusion or interdiffusion experiments and from measurements of the thermal equilibrium concentration of vacancies in the alloy.

From Eqs. (1)–(6) and (8)–(12), we may define partial diffusion coefficients for the various species as follows:

$$D_v = d_{Av} C_A + d_{Bv} C_B, \quad (13)$$

$$D_i = d_{Ai} C_A + d_{Bi} C_B, \quad (14)$$

$$D_A = d_{Av} C_v + d_{Ai} C_i, \quad (15)$$

and

$$D_B = d_{Bv} C_v + d_{Bi} C_i. \quad (16)$$

With the aid of the diffusion coefficients, we can now write the three coupled partial differential equations which describe the time and space dependences of the defect concentrations and the composition of the alloy:

$$\begin{aligned} \frac{\partial C_v}{\partial t} = & \nabla [-(d_{Av} - d_{Bv}) C_v \nabla C_A + D_v \nabla C_v] \\ & + pK_0 - K_{iv} C_i C_v - K_{sv} C_v C_s, \\ \frac{\partial C_i}{\partial t} = & \nabla [(d_{Ai} - d_{Bi}) C_i \nabla C_A + D_i \nabla C_i] \\ & + pK_0 - K_{iv} C_i C_v - K_{si} C_i C_s, \end{aligned} \quad (17)$$

and

$$\frac{\partial C_A}{\partial t} = \nabla [D_A \nabla C_A + C_A (d_{Ai} \nabla C_i - d_{Av} \nabla C_v)].$$

K_0 is the defect production rate and p is the efficiency

factor which takes into account that only a fraction of the defects produced in a cascade will escape spontaneous recombination and clustering and contribute to the RIS. Hence, the product pK_0 is the effective production rate for freely migrating defects.

Defect losses to internal sinks are approximated by the usual rate theory expressions.¹⁵ The terms K_{iv} , K_{sv} , and K_{si} are the rate coefficients for mutual recombination and for the annihilation of vacancies and interstitials at internal sinks, which are assumed to be inexhaustible and randomly distributed. The rate coefficients are approximated by

$$K_{iv} = (16\pi/a_0^3)r_{iv}(D_i + D_v), \quad (18)$$

$$K_{sv} = (16\pi/a_0^3)r_{sv}D_v, \quad (19)$$

and

$$K_{si} = (16\pi/a_0^3)r_{si}D_i. \quad (20)$$

Here r_{iv} is the radius of the recombination volume, and r_{sv} and r_{si} are the trapping radii of solute atoms for vacancy and interstitial defects, respectively.

We note that the set of coupled differential equations (17) cannot be solved in a simple, analytical way. The detailed time and space dependences of the defect and alloy concentrations can be determined numerically. However, some qualitative conclusions can be derived from Eq. (17) by assuming steady state has been achieved. At steady state, the following relation between ∇C_A and ∇C_v holds:

$$\nabla C_A = \frac{C_A C_B d_{Bi} d_{Bv}}{d_{Bi} C_B D_A + d_{Ai} C_A D_B} \left[\frac{d_{Av}}{d_{Bv}} - \frac{d_{Ai}}{d_{Bi}} \right] \nabla C_v. \quad (21)$$

From Eq. (21) it is evident that the relation between the direction of the steady-state gradient of alloy component A and that of the vacancy gradient is determined by the relative magnitudes of the ratios d_{Av}/d_{Bv} and d_{Ai}/d_{Bi} , which are essentially the ratios of the "effective" jump frequencies of A and B atoms into neighboring vacancies, and that of A and B interstitials, respectively. These jump frequencies may contain terms accounting for preferential association of interstitials and/or vacancies with A or B atoms as discussed above. During irradiation, the defect concentrations always decrease toward a defect sink, and Eq. (21) predicts that the element A becomes enriched at sinks if $d_{Ai}/d_{Bi} > d_{Av}/d_{Bv}$. Furthermore, it is evident that, at steady state, the gradient of the alloying elements is an image of the defect gradient in the vicinity of a sink. This implies, for example, that the maximum depth of A -atom (or B -atom) enrichment achieved by the preferential transport of one component to a sink is determined by the depth of the defect profiles at steady state.

For a monoatomic solid, the steady-state distribution of mobile point defects under irradiation has been calculated by Lam, Rothman, and Sizmann.¹⁶ Although in an A - B alloy these results are expected to be modified by the spatial variation of the defect diffusion coefficients and the coupling of the defects to the alloying elements (Kirkendall effect), it is likely that qualitative features will be

maintained. Thus, for the later discussion of our results it is helpful to cite one relation given by Lam *et al.*¹⁶ For the case of mutual recombination being dominant over defect annihilation at internal sinks, i.e., the width of the defect profile at half of its maximum (X_{FWHM}), is given by

$$X_{FWHM} \approx 0.4 \left[\frac{D_v a_0^3}{8\pi p K_0 r_{iv}} \right]^{1/4}. \quad (22)$$

III. EXPERIMENTAL PROCEDURE

Alloys containing 10- and 60-at. % Cu were prepared by arc melting and subsequent levitation melting in an induction furnace. Several 3-mm disks were punched from ~ 0.25 -mm foils rolled from this stock. The disks were annealed in a vacuum of $\sim 10^{-6}$ Pa for 3 h at 850°C, water quenched to room temperature, metallographically polished to obtain an optically flat surface, and then electropolished in a cold solution of 30-vol % HNO₃ and 70-vol % methanol to remove the cold-worked surface layer.

The irradiations were done at the Argonne National Laboratory Dual-Ion Irradiation Facility with 3-MeV ⁵⁸Ni⁺, and in one case with 2.2-MeV Ar⁺ ions. For details of the irradiation procedure we refer to Ref. 17. During bombardment the vacuum pressure was in the 10^{-6} Pa range. Thermocouples were used to monitor and control the temperature of the specimen holder. Individual specimen temperatures were measured during irradiation with a calibrated infrared pyrometer with a relative accuracy of about $\pm 2^\circ\text{C}$. The uncertainty of the temperature measurement, including systematic errors from the calibration, is estimated to be smaller than $\pm 10^\circ\text{C}$. Defect production profiles were calculated from the measured ion energy and current density using a displacement threshold of 40 eV and the Brice codes RASE3 and DAMG2.¹⁸ The peak damage rate was $\sim 2.7 \times 10^{-3}$ displacements per atom per second (dpa/s), and was located at a depth of ~ 500 nm for 3-MeV Ni⁺ ions, and at ~ 700 nm for 2.2-MeV Ar⁺ ions. Near the surface, the displacement rate for both ions was $\sim 1 \times 10^{-3}$ dpa/s. All displacement rates and doses given further in this paper refer to the near-surface region. We note that some sputtering will occur during the elevated-temperature irradiation with high-energy ions. However, the sputtering rate is very low. Less than 3 nm is removed by sputtering during a 5000-s irradiation to 5 dpa. Hence, no significant change in surface composition due to sputtering will occur at elevated temperatures.

AES with low-energy ion sputtering has been employed to determine concentration versus depth profiles. An ~ 100 - μm -diam electron beam of 3 kV and 5 μA was used as the excitation beam. Analysis was performed with Auger electrons of Cu at 920 eV, and Ni at 716 eV. Conversion of AES peak-to-peak ratios to alloy compositions was based on the results of Goto *et al.*¹⁹ For depth profiling, a 70- $\mu\text{A}/\text{cm}^2$ beam of 2-kV Ar⁺ ions was used to sputter ~ 2 -mm-diam areas of the specimens. The sputtering rates for the alloys are slightly concentration dependent. Calculations from published sputtering yields²⁰ give steady-state values of 0.14 nm/s for the

Ni-10 at. % Cu alloy and 0.17 nm/s for the Ni-60 at. % Cu alloy.

IV. EXPERIMENTAL RESULTS

Both alloys, Ni-10 at. % Cu and Ni-60 at. % Cu, were irradiated with 3-MeV Ni ions to three different doses at five different temperatures from 422 to 610°C. The lowest dose was ~ 0.20 dpa, the next was ~ 1.2 dpa, and the highest one, ~ 5.0 dpa. For an irradiation series to different doses at a given temperature, three specimens of each alloy were mounted side by side on the same heating stage. Starting with the irradiation of the high-dose specimen, the specimens were successively exposed to the beam by stepwise removing the shielding mask. Owing to their different positions on the heating stage, the temperatures of the three specimens differed within a range of $\pm 5^\circ\text{C}$. Since these differences are comparatively small, each dose series is labeled further in this paper by only the average temperature.

Figures 1 and 2 show concentration versus depth profiles obtained by AES from Ni-60 at. % Cu and Ni-10 at. % Cu specimens after irradiation to the highest doses attained at several temperatures, along with two profiles from unirradiated control specimens which were mounted in the irradiation rig but shielded from the bombarding ions. Since Auger electrons of the transitions used for the analysis have a mean escape depth of ~ 1.5 nm, the compositions indicated on the right-hand ordinate represent an average over several atom layers. In all specimens, the peak-to-peak heights of the major surface contaminants, C and O, were reduced to background levels after < 30 s of

sputtering. The depth profiles from the control specimens exhibit the behavior expected when sputter-profiling Ni-Cu specimens whose compositions do not vary as a function of depth. Preferential removal of copper atoms during sputtering causes the initial sharp drop seen in the Auger ratios. By a quantitative consideration of the different sputtering yields for nickel and copper,²¹ steady-state Auger ratios representing 48 at. % Cu are expected for a 60-at. % Cu alloy, and 7 at. % Cu for a 10-at. % Cu alloy.

To convert AES profiles as presented in Figs. 1 and 2 to concentration versus depth profiles which is necessary for a quantitative evaluation, we make the following assumptions:

(1) We assume the sputtering rate to be constant during the entire sputtering process of a specimen, i.e., 0.17 nm/s for the 60-at. % Cu alloy and 0.14 nm/s for the 10-at. % Cu alloy. This approximation is reasonable since the variations in sputtering rate due to compositional changes are about $\pm 6\%$ for the observed concentration variations.²⁰

(2) It is assumed that sputtering during depth profiling is always close to steady state. That is, the composition determined from the measured AES ratios is assumed to be proportional to the specimen composition at the corresponding depth without sputtering. From the profiles of the control specimens we see that steady state is achieved relatively fast, i.e., within 20–30 s of sputtering. Hence, this assumption appears reasonable except for the very-near-surface region, i.e., for the first 3–5 nm in depth.

The depth profiles in Fig. 1 reveal that in the irradiated specimens the copper concentrations in the near-surface regions are considerably less than those in the control

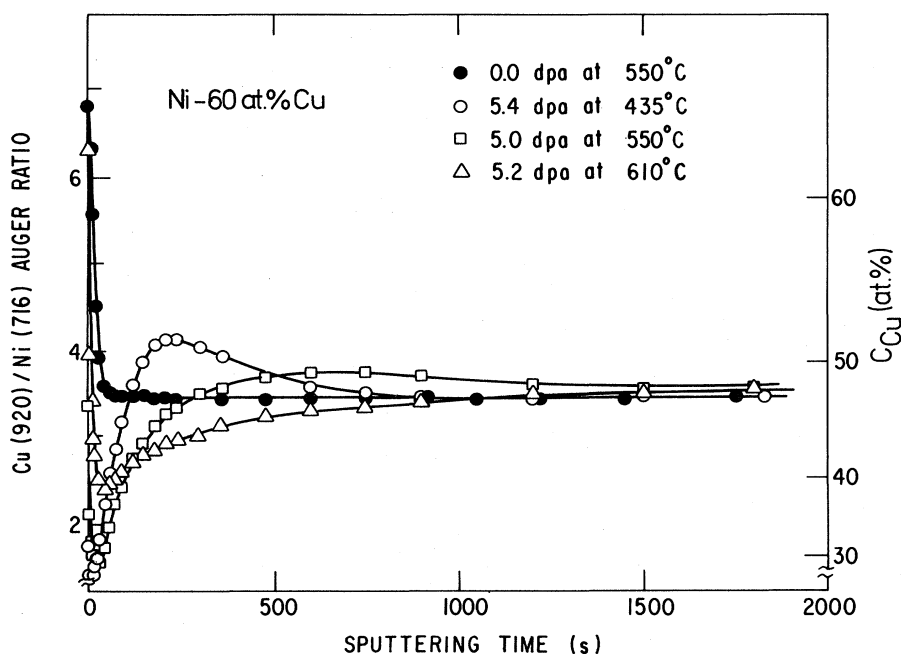


FIG. 1. AES depth profiles of the Cu concentration for three Ni-60 at. % Cu specimens irradiated with 3-MeV Ni⁺ ions to a dose of ~ 5 dpa at different temperatures, along with the depth profile of an unirradiated control specimen.

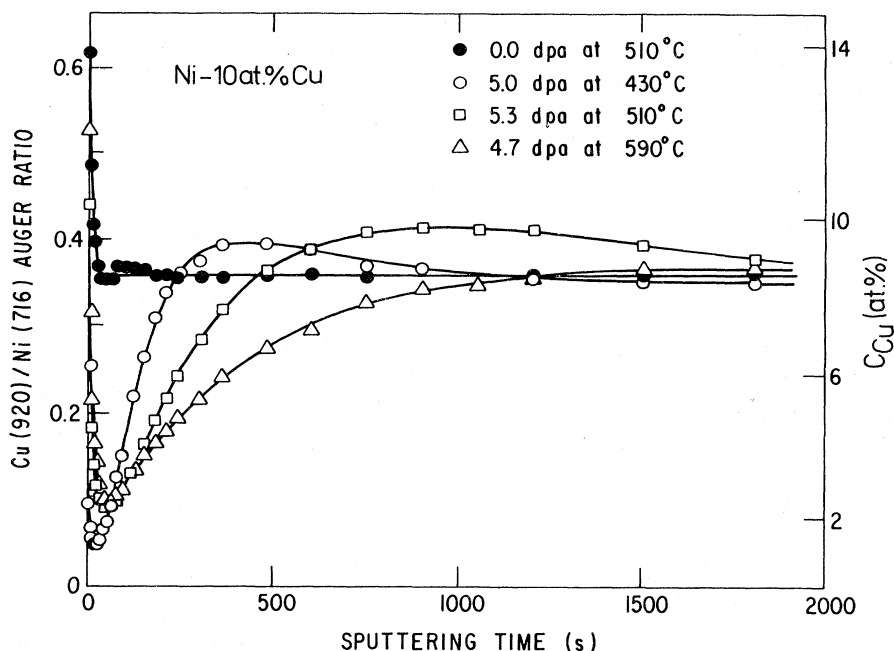


FIG. 2. As for Fig. 1, but for Ni-10 at. % Cu.

specimen. Irradiation at elevated temperatures has produced a Cu-depleted (Ni-enriched) region at the irradiated surface. Beneath this region, the copper concentrations of the irradiated specimens increase above the steady-state value of the control specimen, indicating a Cu-enriched (Ni-depleted) region at intermediate depths. Compared to the near-surface Cu depletion, this increase in Cu concentration is less significant (only a few at. %) but broader in distribution. Deep in the specimens, the Cu composition decreases to a steady-state value after sputtering of (48 ± 1) at. % Cu. In the specimen irradiated at 610°C the approach to the steady-state sputtered composition occurs at ~ 3000 s of sputtering (which corresponds to a depth of ~ 500 nm), and is not shown in Fig. 1.

Similar to the observations in the Ni-60 at. % Cu alloys, the irradiated Ni-10 at. % Cu specimens (Fig. 2) also show a Cu-depleted (Ni-enriched) surface layer accompanied by Cu enrichment at intermediate depths. The temperature dependence of the profiles is similar to that of Fig. 1, i.e., the width of the Cu-depleted layer increases with increasing irradiation temperature. However, the Cu depletion extends significantly deeper into the Ni-10 at. % Cu specimens at corresponding temperatures and doses than into the Ni-60 at. % Cu specimens.

All measured AES depth profiles from irradiated specimens, illustrating the dose dependence of the RIS at five different irradiation temperatures, are shown in Fig. 3(a) for the Ni-60 at. % Cu alloy and in Fig. 4(a) for the Ni-10 at. % Cu alloy. Profiles from unirradiated control specimens are not included in Figs. 3 and 4 to avoid overcrowding the figures. The control profiles shown in Figs. 1 and 2 are representative for all profiles shown in Figs. 3

and 4. We note that each profile is taken from a different specimen and thus may be influenced by differences in texture, orientation, or other specimen specific features. For example, variations of the determined bulk concentration in the limits of ± 1 at. % are frequently observed, and in some cases, these limits are exceeded. The measured profiles have not been corrected for such effects.

Figure 5 presents results which demonstrate that the segregation effects are radiation induced, rather than radiation enhanced. A process is described as being radiation enhanced when equilibrium is approached at an enhanced rate during irradiation. Radiation induced describes processes which revert in the absence of irradiation. The depth profile of a specimen in the as-prepared, electropolished condition and the profiles of two other specimens which were irradiated with 2.2-MeV Ar^+ to the same dose (5 dpa), at the same temperature (500°C) and dose rate ($\sim 1 \times 10^{-3}$ dpa/s) are shown in Fig. 5. One specimen was depth profiled in the as-irradiated condition; the second was subsequently annealed for 100 h at the temperature at which it had been irradiated, then depth profiled.

Both the as-irradiated specimen and the irradiated and annealed specimen show a Cu-depleted surface layer accompanied by copper enrichment at intermediate depths. However, annealing at the irradiation temperature has significantly reduced the amount of segregation. This result demonstrates that the Cu depletion at the surface is thermodynamically unstable at the irradiation temperature and hence, is radiation induced.

The annealing results presented in Fig. 5 also show the influence of thermal backdiffusion at the irradiation tem-

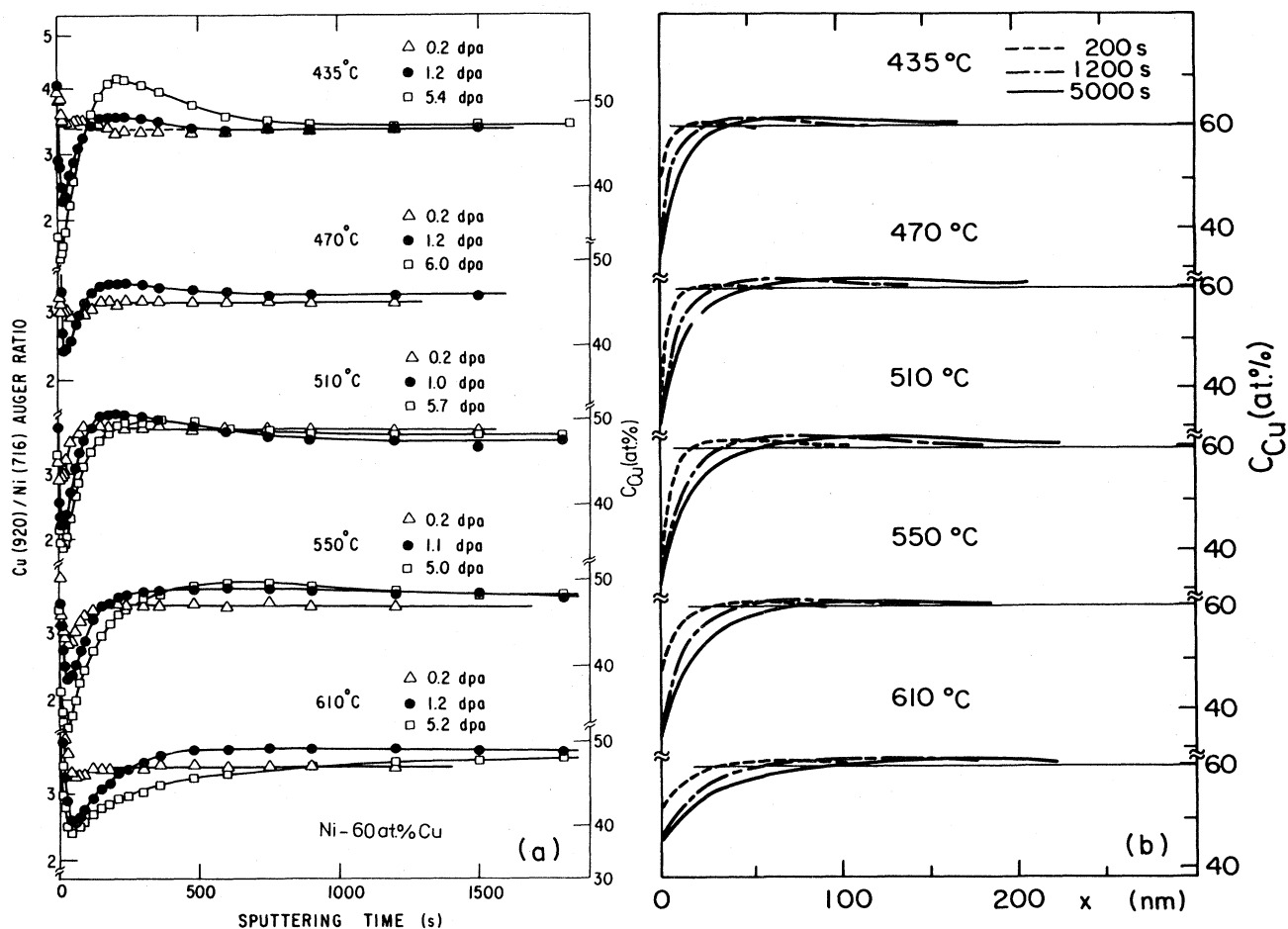


FIG. 3. Dose and temperature dependence of the near-surface Cu concentration in Ni-60 at. % Cu alloys after irradiation with 3-MeV Ni^+ ions. (a) Measured AES depth profiles. The given doses are based on a calculated dose rate of 1×10^{-3} dpa/s. (b) Calculated AES depth profiles for the corresponding irradiation times and temperatures using the parameters listed in Tables I and II.

perature. At 500°C the influence of *thermal* backdiffusion is relatively low; 100 h of annealing is not enough to remove the segregation established during only ~ 1 h of irradiation. However, diffusion during irradiation will be significantly enhanced by the presence of radiation-induced defects. This enhancement during irradiation has been found to be particularly efficient in NiCu alloys.¹³ Therefore, backdiffusion during bombardment will be much larger than that during thermal annealing at the same temperature.

To examine whether the reduction of segregation during the annealing at 500°C is due to normal thermal backdiffusion, depth profiles after annealing have been calculated using Fick's second law and the as-irradiated depth profile as the starting profile. To avoid complications, sputter-induced compositional changes have been neglected. Results of the calculations for three different values of the interdiffusion coefficient \tilde{D} are presented in Fig. 5. By comparison with the experimentally determined concentration profile, the interdiffusion coefficient for the temperature of 500°C can be determined as

$$\tilde{D} = (1.4_{-0.5}^{+1.4}) \times 10^{-17}$$

measured in cm^2/s . For a comparison of this value with literature data we refer to Fig. 10 and the later discussion.

V. NUMERICAL CALCULATIONS

The aim of this section is to obtain solutions of the system of partial differential equations (17) which fit the experimental data presented in Figs. 3 and 4. Since general analytical solutions do not exist, there is no straightforward method for fitting Eqs. (17) to the data. The procedure we have adopted is to obtain numerical solutions for the given experimental conditions with a particular set of defect parameters. The calculations are repeated with systematically varied input parameters until the results fit the data satisfactorily. This fitting procedure is an empirical trial-and-error procedure. The experimental parameters are the irradiation time, the irradiation temperature, and the bulk alloy composition.

In the following, the index *A* refers to copper and the

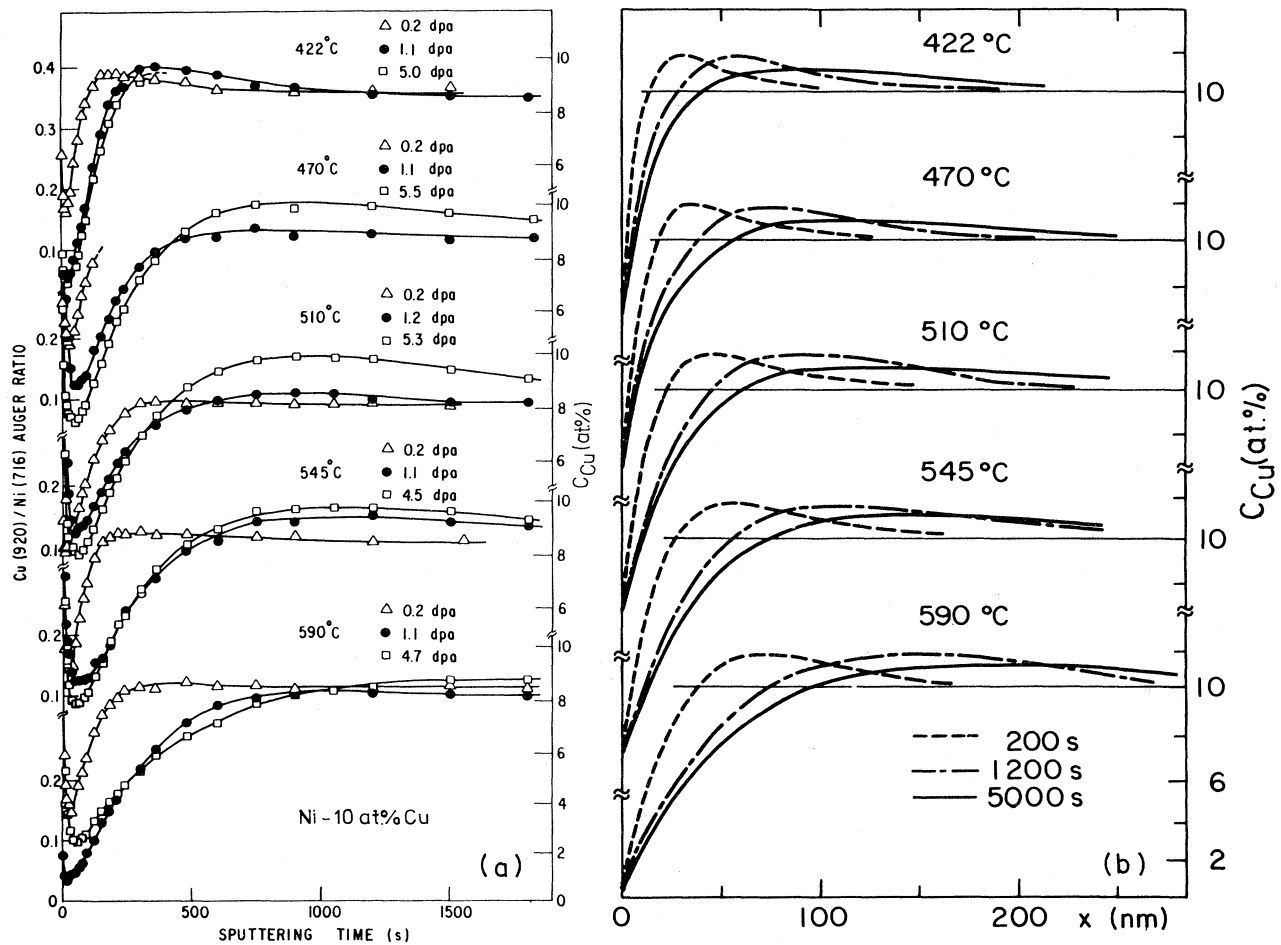


FIG. 4. As for Fig. 3, but for Ni-10 at. % Cu.

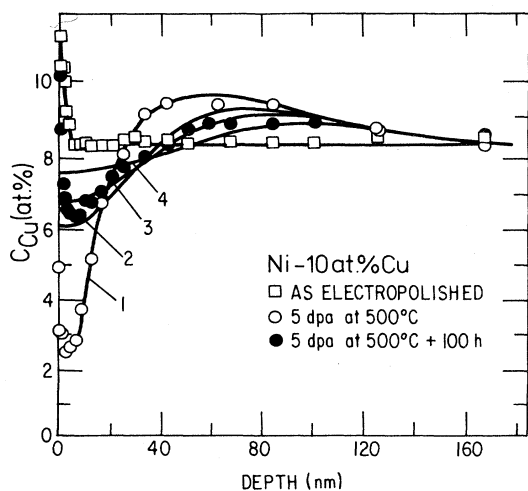


FIG. 5. AES depth profiles of the Cu concentration for three Ni-10 at. % Cu specimens, one "as-prepared," one irradiated at 500°C with 2.2-MeV Ar⁺ to 5 dpa, and one after irradiation and annealing for 100 h at 500°C. Solid lines correspond to concentration profiles calculated according to Fick's second law with interdiffusion coefficients of $\bar{D}=0.9 \times 10^{-17}$ cm²/s (2), 1.4×10^{-17} cm²/s (3) and 2.8×10^{-17} cm²/s (4), and starting with a concentration profile equal to (1).

index B to nickel. Numerical solutions of the system of partial differential equations, Eqs. (17), were obtained for a thin foil by means of the GEAR package of subroutines²² starting from thermodynamic equilibrium conditions. The foil thickness used was $L=2500$ nm. Since this thickness is significantly greater than the range of observed concentration modifications, the foil geometry is a good approximation for a semiinfinite bulk specimen. Conditions at the boundaries, i.e., at the surface and at the foil center ($x = \frac{1}{2}L$), all concentration gradients were set equal to zero:

$$\frac{\partial C_i(t, \frac{1}{2}L)}{\partial x} = \frac{\partial C_v(t, \frac{1}{2}L)}{\partial x} = \frac{\partial C_A(t, \frac{1}{2}L)}{\partial x} = 0, \quad (23)$$

whereas at the foil surface ($x=0$), the concentrations of interstitials and vacancies were fixed at their thermal equilibrium values,

$$C_i(t, 0) = \exp(S_i^f/k) \exp(-H_i^f/kT), \quad (24)$$

and

$$C_v(t, 0) = \exp(S_v^f/k) \exp(-H_v^f/kT), \quad (25)$$

where H_i^f and H_v^f are the formation enthalpies of intersti-

tials and vacancies in the alloy and S_v^f and S_i^f the effective formation entropies. The missing boundary condition at the foil surface, i.e., the surface concentration of copper, was replaced by the conservation condition

$$\int_0^{L/2} C_A(t,x)dx = \frac{1}{2} C_A^0 L, \quad (26)$$

where C_A^0 is the initially uniform concentration of copper. The set of fixed input parameters for the numerical calculations is listed in Table I, and the choices are discussed in the following section. These parameters have been kept unchanged for the fitting procedure. They are assumed to be independent of temperature (in the range from 420 to 610°C), irradiation dose, and spatial coordinates. Furthermore, the parameters are assumed to be the same for both alloys, unless different values are explicitly known, e.g., for a_0 .²³

In Table II, the parameters are listed which were systematically varied during the fitting procedure to obtain the desired coincidence of the calculated and the experimentally determined profiles; here as well the assumption was made that the parameters are independent of temperature, dose, and spatial coordinates. The effects of varying the parameters in Table II on the calculated concentration profiles are discussed in detail in the discussion (Sec. VI). The values of H are known to depend to a degree on the composition and, therefore, on spatial coordinates. However, to a first approximation it is reasonable to assume that these parameters are spatially uniform in each alloy. The sink density, recombination radius, and defect production efficiency are taken equal for both alloys. The numerical solutions of Eqs. (17) with the parameters of Tables I and II are shown in Figs. 3(b) and 4(b), for the 60-at. % Cu alloy and for the 10-at. % Cu alloy, respectively. The scales were kept identical with those of Figs. 3(a) and 4(a) to facilitate direct comparison.

VI. DISCUSSION

From the depth profiles presented in Figs. 1 to 5 it is apparent that during irradiation at temperatures between 420 and 610°C, a significant Ni enrichment (Cu depletion)

occurs in both alloys at the irradiated surface, accompanied by a Ni-depleted region at intermediate depth. As shown by the annealing experiment presented in Fig. 5, this segregation is induced by the irradiation, i.e., non-equilibrium in nature, and cannot be due to the enhancement of normal diffusion processes during irradiation. Hence, the fluxes of vacancies and/or interstitials toward the surface are accompanied in both alloys by a nonbalanced flux of the alloying elements. Considering Eq. (21), our results imply that

$$d_{Cu,v}/d_{Ni,v} > d_{Cu,i}/d_{Ni,i}.$$

Consequently, either vacancies diffuse faster via the Cu atoms than the Ni atoms, or interstitials diffuse faster via the Ni atoms, or both.

We would like to specify some additional qualitative features of the observed segregation which can be deduced directly from Figs. 1–4:

(1) In both alloys, the width of the Ni-enriched (Cu-depleted) surface layer increases with increasing dose. Typical Ni-enriched layer thicknesses at 5 dpa are 10 to 100 nm.

(2) At the same dose, the resulting concentration gradients in both alloys are steeper at lower temperatures.

(3) For equivalent doses, the radiation-induced concentration gradients extend deeper into the Ni–10 at. % Cu specimens than into the Ni–60 at. % Cu specimens.

(4) The Ni–10 at. % Cu alloy exhibits strong Cu depletion (from 10 to ≤ 2 at. %) in the near-surface region, while the relative change in the 60-at. % Cu alloy is less (from 60 to ~ 40 at. %).

(5) The profiles from the 60-at. % Cu alloy are still changing significantly between 1 and 5 dpa, while the changes in the 10-at. % Cu alloy are much less over the same dose range. That is, at the higher doses, the more dilute alloy appears closer to attaining steady state.

All these features are reproduced in the calculated concentration profiles [Figs. 3(b) and 4(b)]. We emphasize that *all* calculated profiles were obtained with a *single* set of input parameters (Tables I and II). Only the activation enthalpies for migration, and those parameters for which

TABLE I. Fixed parameters.

	Parameter	10-at. % Cu	60-at. % Cu	Source
Defect formation entropies and enthalpies	S_v^f	3k	3k	Assumed
	S_i^f	0	0	Assumed
	H_v^f	1.60 eV	1.41 eV	Refs. 30 and 32, linear concentration interpol.
	H_i^f	4.0 eV	4.0 eV	Assumed
Lattice constant	a_0	0.352 nm	0.357 nm	Ref. 22
Sink radii	r_{sv}, r_{si}	0.3 nm	0.3 nm	Assumed
Frequency factors	ν_{Av}^0, ν_{Bv}^0	$5 \times 10^{13} \text{ s}^{-1}$	$5 \times 10^{13} \text{ s}^{-1}$	Assumed
	ν_{Ai}^0, ν_{Bi}^0	$5 \times 10^{13} \text{ s}^{-1}$	$5 \times 10^{13} \text{ s}^{-1}$	Assumed
Defect production rate	K_0	$1 \times 10^{-3} \text{ dpa/s}$	$1 \times 10^{-3} \text{ dpa/s}$	Calculated Ref. 18

TABLE II. Derived parameters for best fit.

	Parameter	10 at. % Cu	60 at. % Cu	
Migration enthalpies (eV)	H_{Av}	1.00	1.06	1.06
	H_{Bv}	1.15	1.12	1.06
	H_{Ai}	0.30	0.20	0.23
	H_{Bi}	0.12	0.20	0.17
Sink density	C_s	$\leq 10^{-8}$	$\leq 10^{-8}$	
Recombination radius	r_{iv}	$0.8a_0$	$0.8a_0$	
Defect production efficiency	p	0.40	0.40	

a concentration dependence is known explicitly, were different for the two alloys.

For further discussion, a quantitative definition of the amount of segregation is useful. For systems like Ni-Cu in which all of the redistributed solute remains in solution, an appropriate quantity has been suggested by Sethi and Okamoto.²⁴ Following their suggestion, we define the amount of segregation to the surface, $\hat{s}(t)$, as

$$\hat{s}(t) = \int_0^{x_0} \left(\frac{C_{Cu}^0}{C_{Ni}^0} - \frac{C_{Cu}(t,x)}{C_{Ni}(t,x)} \right) dx, \quad (27)$$

where $C_{Cu}(t,x)$ and $C_{Ni}(t,x)$ are the concentrations of Cu and Ni atoms after an irradiation time, t , as a function of depth, x , from the surface. C_{Cu}^0 and C_{Ni}^0 are the initial, uniform bulk concentrations. The integration is performed from the surface to the depth x_0 , where the measured concentration crosses the bulk concentration, i.e.,

$C_{Cu}(t,x_0) = C_{Cu}^0$. The quantity $\hat{s}(t)$ is a measure of the number of Cu atoms per unit area that has been transported from the surface region ($0 \leq x \leq x_0$) into the interior ($x \geq x_0$). As is evident from Figs. 1 to 4, the location of x_0 is not fixed, but depends both on time and temperature.

The $\hat{s}(t)$'s determined from the depth profiles in Figs. 3(a) and 4(a) are plotted in Figs. 6(a) and 6(b) as a function of the square root of the irradiation time. In addition, the dose dependences as calculated from Eq. (17) with the parameters listed in Tables I and II are also plotted (solid lines). The calculated dose dependences satisfactorily follow the experimentally determined values. According to Eq. (21), the concentration gradient of Cu atoms in steady state is determined by the vacancy concentration gradient. At the very beginning of the irradiation, all defect and alloy concentration gradients are zero, causing $\hat{s}(t)$ to start with zero slope. For later irradiation times, the rate of segregation slows because of the continual approach of

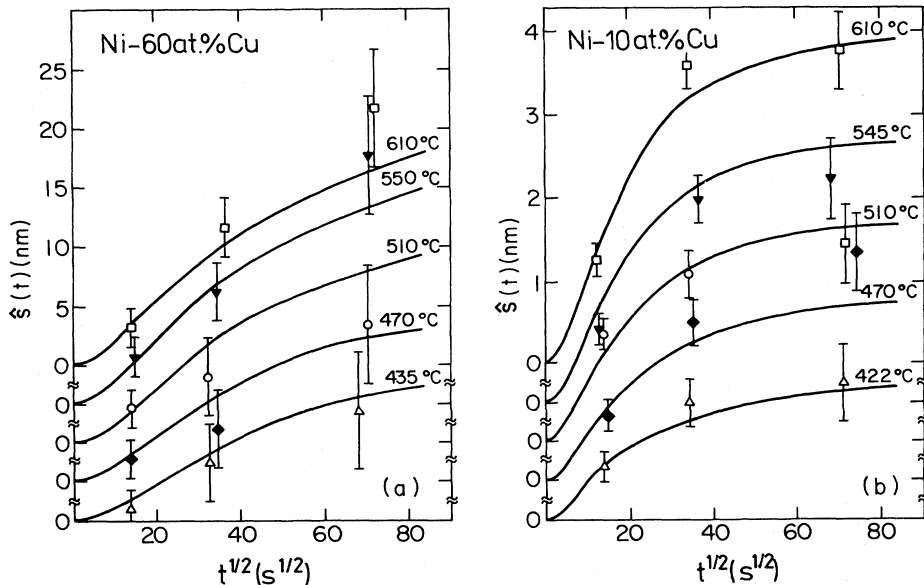


FIG. 6. The dependence of the amount of segregation, \hat{s} , on the irradiation time in (a) Ni-60 at. % Cu and (b) Ni-10 at. % Cu. The graph shows values determined experimentally from the AES depth profiles, and the time dependences calculated using the parameters of Tables I and II (solid lines). Note the square-root scaling at the abscissa.

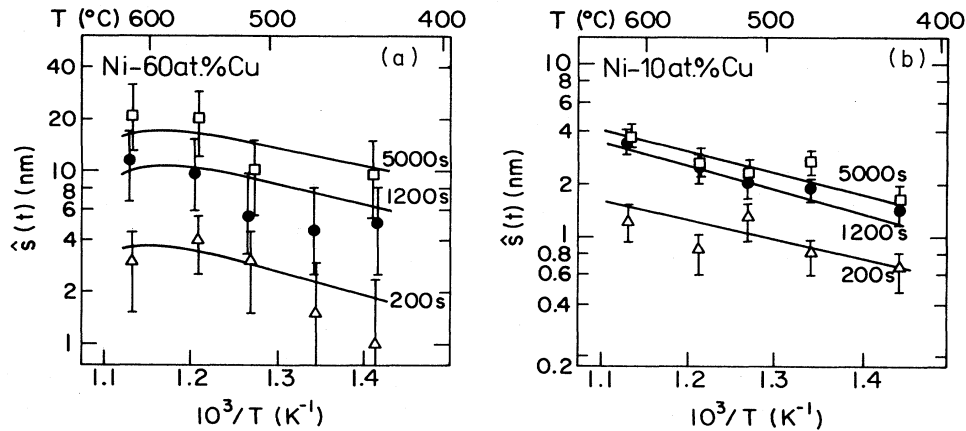


FIG. 7. Arrhenius plot of the amount of segregation, \hat{s} , in Ni-60 at. % Cu (a) and Ni-10 at. % Cu (b), as determined experimentally from the AES depth profiles and as calculated for the corresponding irradiation times using the parameters of Tables I and II (solid lines).

∇C_A to ∇C_v . This slowing of the segregation is most obvious in the Ni-10 at. % Cu alloy [Fig. 6(b)].

The temperature dependence of $\hat{s}(t)$ is shown in Figs. 7(a) and 7(b), where the measured data points and calculated solid lines are plotted in Arrhenius graphs. The effective activation enthalpies H_{eff} are listed in Table III. The values of $H_{\text{eff}}^{\text{calc}}$ were obtained from the slopes of the lines in Fig. 7, ignoring the curvature at high temperatures in the 60-at. % Cu alloy. The experimental values were obtained by a least-squares fit to the data points assuming H_{eff} to be constant during the irradiation and independent of irradiation temperature. According to Eq. (22), the amount of segregation should be proportional to $D_v^{1/4}$, assuming that the vacancy concentration profiles in the alloys have the same approximate dependence as in pure metals. Since $D_v = d_{Av}C_A + d_{Bv}C_B$, the values of H_{eff} are expected to be about $\frac{1}{4}$ of the vacancy migration energy, which indeed is reproduced by our results within the limits of uncertainty (cf. Table III).

Although the theoretical model was kept as simple as possible, the number of physical parameters which enter the calculations is fairly large (cf. Tables I and II). Many of these parameters are not precisely known, and a number of assumptions was necessary to reduce the spectrum of possible parameter variations. Therefore, a critical dis-

cussion of the input parameters will be given next.

The parameters in Table I are either well known, or the calculations are not very sensitive to variations of these parameters within reasonable limits. S^f and H^f determine the thermal-equilibrium defect concentrations, which are negligibly small compared to the radiation-induced defect concentrations in the present experiments. The pre-exponential factors were assumed to be the same for all defect species and independent of composition, and were chosen to yield a calculated tracer diffusion coefficient for Cu atoms at 500°C which coincides with the value determined from our backdiffusion experiment.

The parameters listed in Table II result from our fitting procedure. They cannot be derived from other available experimental results with the required accuracy. It is necessary to critically scrutinize these input parameters, since they are the ones that predominantly affect the segregation kinetics. Systematic parameter variations were performed to determine the quantitative influence on the segregation profiles. For this procedure, each of the parameters in Table II was varied in a reasonable range while all other parameters were kept fixed to their "best-fit" values. In the following, the results of such parameter variations are discussed. The indicators chosen are the amount of segregation for the highest dose, $\hat{s} = \hat{s}(5000 \text{ s})$,

TABLE III. Effective activation enthalpies (in eV) of the segregation process determined from the calculations ($H_{\text{eff}}^{\text{calc}}$), and by a least-squares fit to the data ($H_{\text{eff}}^{\text{exp}}$) in comparison with $\frac{1}{4}$ of the migration enthalpy of the slower moving defect species (vacancies).

t_{irr} (s)	Ni-10 at. % Cu				Ni-60 at. % Cu			
	$H_{\text{eff}}^{\text{calc}}$	$H_{Av}/4$	$H_{Bv}/4$	$H_{\text{eff}}^{\text{exp}}$	$H_{\text{eff}}^{\text{calc}}$	$H_{Av}/4$	$H_{Bv}/4$	$H_{\text{eff}}^{\text{exp}}$
200	0.23				0.27			
1200	0.27	0.25	0.29	0.22±0.05	0.22	0.26	0.28	0.27±0.05
5000	0.25				0.20			

and the rate of approach to steady state, characterized by $S \equiv \hat{s}(1200 \text{ s})/\hat{s}(5000 \text{ s})$.

We first consider the sink density parameter $C_s r_s$. For $C_s r_s \geq 10^{-8}$ nm, in both alloys \hat{s} is severely reduced with increasing sink density. For $C_s r_s \geq 10^{-6}$ nm virtually no segregation is expected. Only for $C_s r_s < 10^{-8}$ nm, which is a typical value for a well-annealed alloy, does \hat{s} reach the experimentally observed quantity. Hence, the effect of radiation-induced sinks is negligible at the irradiation temperatures and for the alloys investigated. This result is in agreement with electron microscope observations of heavy ion bombardment of pure Ni and Cu specimens, which revealed that the number of visible loops decreases sharply at temperatures above 300°C in Cu (Ref. 25) and above 500°C in Ni,²⁶ due to the thermal emission of vacancies.

The recombination radius r_{iv} was chosen as follows. Any smaller value than the selected $0.8a_0$ for r_{iv} would not be realistic, since this is approximately the nearest-neighbor distance ($a_0/\sqrt{2}$). Although in this case a treatment of the recombination reaction using lattice theory would seem to be appropriate, Schröder and Eberlein²⁷ have shown that the continuum treatment¹⁵ is a good approximation even for small recombination radii. The calculations reveal that for increasing r_{iv} the amount of segregation is reduced, deviating more and more from the experimentally observed quantity. Attempts to compensate for this reduction by varying other parameters proved difficult, and soon brought the other parameters out of reasonable limits. From damage-rate measurements at low temperatures, r_{iv} has been determined as a function of temperature for pure Cu by Lennartz *et al.*²⁸ Extrapolating their values to the temperature of 510°C yields $r_{iv} = (1.6_{-0.8}^{+2.0})a_0$. For $1.6a_0$, all efforts to compensate for the reduced \hat{s} and S values failed. However, the selected value ($r_{iv} = 0.8a_0$) is within the limits of uncertainty determined from the measurements of Lennartz *et al.*²⁸

The dependences of \hat{s} and S on the effective defect-production rate (pK_0) are shown graphically in Fig. 8 for a temperature of 510°C. The experimental results are best reproduced by a value of 4×10^{-4} dpa/s. Using the calculated K_0 of 1×10^{-3} dpa/s, the defect-production efficiency, p , is 0.4, i.e., 40% of the calculated number of defects escape the cascade volume and contribute to long-range material transport. One interesting aspect is that in a wide range of pK_0 , the amount of segregation decreases with increasing pK_0 , even if the segregation is calculated for the same irradiation time, not dose. This is most obvious in Fig. 8(b) (Ni–10 at. % Cu), but also in Fig. 8(a) (Ni–60 at. % Cu) for $pK_0 > 5 \times 10^{-4}$ dpa/s. According to Eq. (22), such behavior is expected near steady state, where $X_{FWHM} \propto (pK_0)^{-1/4}$.

The dependence on the migration enthalpies (H_{Av} , H_{Bv} , H_{Ai} , and H_{Bi}) is complex, and these variables are not independent. Since general rules have not been obtained, we will demonstrate tendencies by means of some specific examples. For further discussion, it is helpful to introduce the differences $\Delta H_v = H_{Bv} - H_{Av}$ and $\Delta H_i = H_{Bi} - H_{Ai}$, since it is these differences which mainly determine the segregation kinetics [cf. Eq. (21)].

Figure 9 demonstrates the segregation dependence in Ni–10 at. % Cu on ΔH_v , for two different values of ΔH_i , namely $\Delta H_i = 0$ (no interstitial contribution to the segregation) and $\Delta H_i = -0.18$ eV (support of the segregation by interstitials). A value of $\Delta H_v \geq 0$ is required to match the experimentally observed value of S , with the most probable value being $0.12 \text{ eV} \leq \Delta H_v \leq 0.18 \text{ eV}$. The fact that a positive ΔH_v is required to fit the experimental results is quite significant, since it implies that preferential transport of copper atoms away from the surface by the vacancy flux is responsible for a significant amount of the observed segregation in the Ni–10 at. % Cu alloy. However, it is also apparent from Fig. 9 that the experimentally observed \hat{s} is not attained for any value of ΔH_v without preferential transport of nickel atoms toward the surface via the interstitial flux, i.e., $\Delta H_i < 0$. A further examination of the segregation dependence on ΔH_i determines that, for constant $\Delta H_v = 0.15$ eV, \hat{s} is increasing with increasing negative values of ΔH_i , and $|\Delta H_i| \geq 0.18$ eV is required to attain the measured \hat{s} . For $|\Delta H_i| > 0.2$ eV no further variation of \hat{s} occurs.

Some pertinent, although indirect, information is available in the literature for checking these values of ΔH_v and ΔH_i . We will discuss the information which is available on vacancies first. Figure 10 summarizes literature data of tracer diffusion coefficients of the Ni–Cu system,^{29–32} extrapolated from the measuring temperature ($\geq 1000^\circ\text{C}$) to a temperature of 500°C. Despite the wide range of extrapolation, it appears likely that the diffusion of copper atoms via vacancies is faster than that of nickel atoms. If we assume that the ratio of the tracer diffusion coefficients, $D_{\text{Cu}}^*/D_{\text{Ni}}^*$, is equal to the ratio of the partial diffusivities, $d_{\text{Cu},v}/d_{\text{Ni},v}$, from Fig. 10 we obtain $d_{\text{Cu},v}/d_{\text{Ni},v} = 12$ for a 10-at. % Cu alloy. The best-fit values for H_{Av} and H_{Bv} from Table II yield $d_{\text{Cu},v}/d_{\text{Ni},v} = 9$, in very good agreement with the value obtained from the literature. The vertical bar marked with an A in Fig. 10 is the value of the diffusion coefficient which was determined from the annealing experiment (Fig. 5) with the 10-at. % Cu alloy at 500°C assuming

$$\tilde{D} = D_{\text{Cu}}^* C_{\text{Ni}} + D_{\text{Ni}}^* C_{\text{Cu}} \approx D_{\text{Cu}}^* C_{\text{Ni}}.$$

The last step follows since $C_{\text{Cu}} = C_{\text{Ni}}/9$, and $D_{\text{Ni}}^* < D_{\text{Cu}}^*$. It, too, agrees well with the extrapolation of the measurements available in the literature. Hence, the best-fit vacancy parameters are in good agreement with the literature.

Some information is also available with which to compare the best-fit interstitial parameters. The activation enthalpy for interstitial migration in pure copper and pure nickel is ~ 0.1 eV.³³ This should be a lower limit for the nickel interstitial in Cu–Ni alloys (recall that the model requires preferential transport of nickel to reproduce the experimental results). Poerschke and Wollenberger¹¹ report an upper limit of 0.25 eV for the activation enthalpy for interdiffusion in a Ni–41 at. % Cu alloy, which serves as an upper limit for the copper interstitial in the present experiments. Since interdiffusion via interstitials requires that the interstitials exchange with both

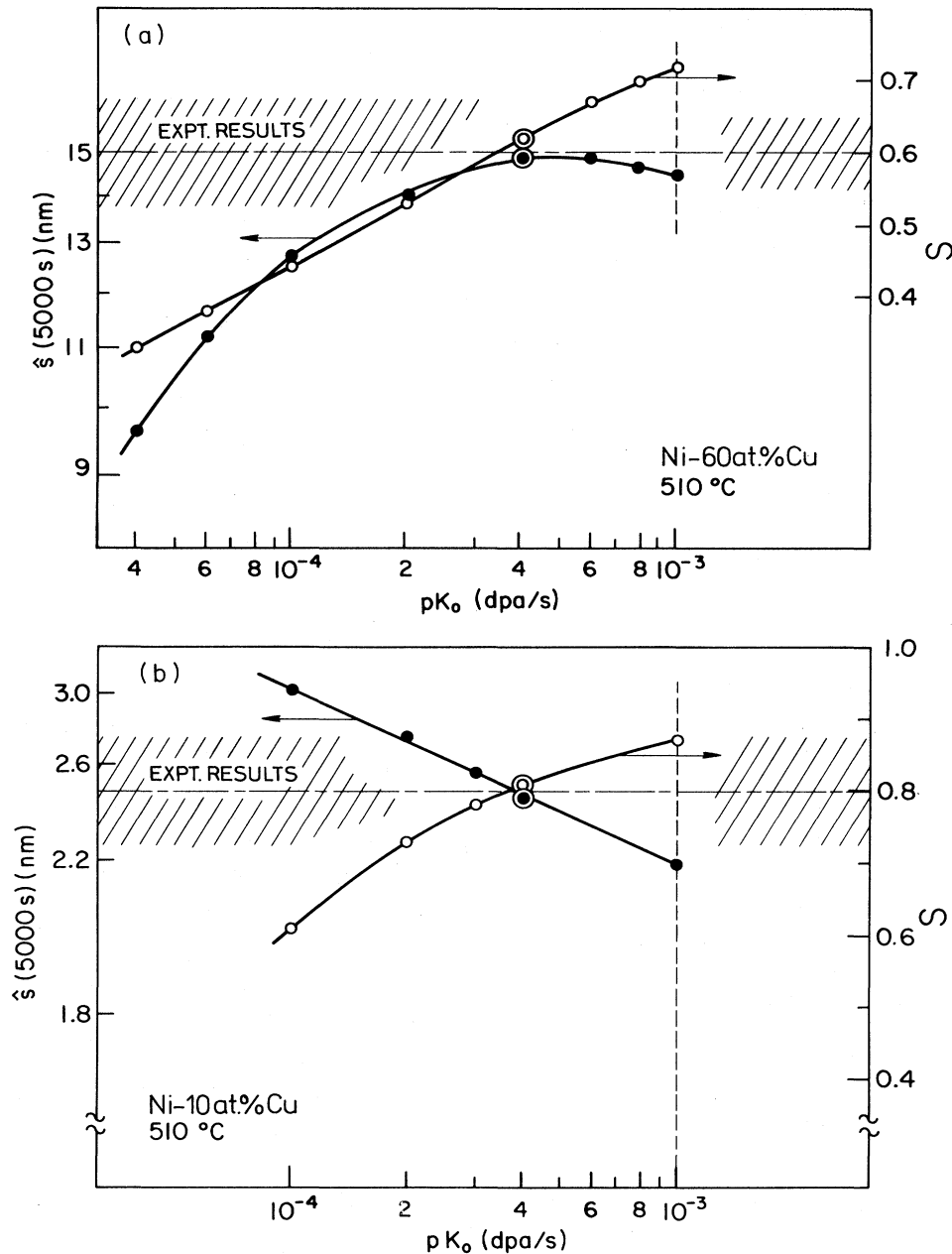


FIG. 8. Example of the dependence of the amount of segregation and of the segregation kinetics on the defect production rate (pK_0) in (a) Ni-60 at. % Cu and (b) Ni-10 at. % Cu, in comparison with the experimental results (shaded region, which applies to the left- and right-hand ordinates). The values (●, ○) were obtained by numerical calculations, based on the parameters given in Tables I and II. The encircled symbols correspond to the entire set given in Table II, including the varied parameter (here pK_0). The lines are drawn as a guide for the eye.

alloy components, the "slower" interstitial will determine the diffusion kinetics. The interstitial parameters in Table II do fall within these limits of 0.1 to 0.25 eV. Note that the definition of an effective migration enthalpy in the model of Wiedersich *et al.*⁶ accounts for any preferential association between interstitials and alloy components.

With respect to the absolute values of the migration

enthalpies the calculations reveal that, for constant $\Delta H_v = 0.15$ eV, the segregation shows a strong dependence on H_{Av} and H_{Bv} . In contrast, for constant $\Delta H_i = -0.18$ eV, \hat{s} and S are virtually independent of H_{Ai} and H_{Bi} in the range $0.02 \text{ eV} \leq H_{Bi} \leq 0.32 \text{ eV}$ and $0.20 \text{ eV} \leq H_{Ai} \leq 0.50 \text{ eV}$. Variations in \hat{s} and S do not occur before H_{Ai} approaches the vacancy migration enthalpy. This insensi-

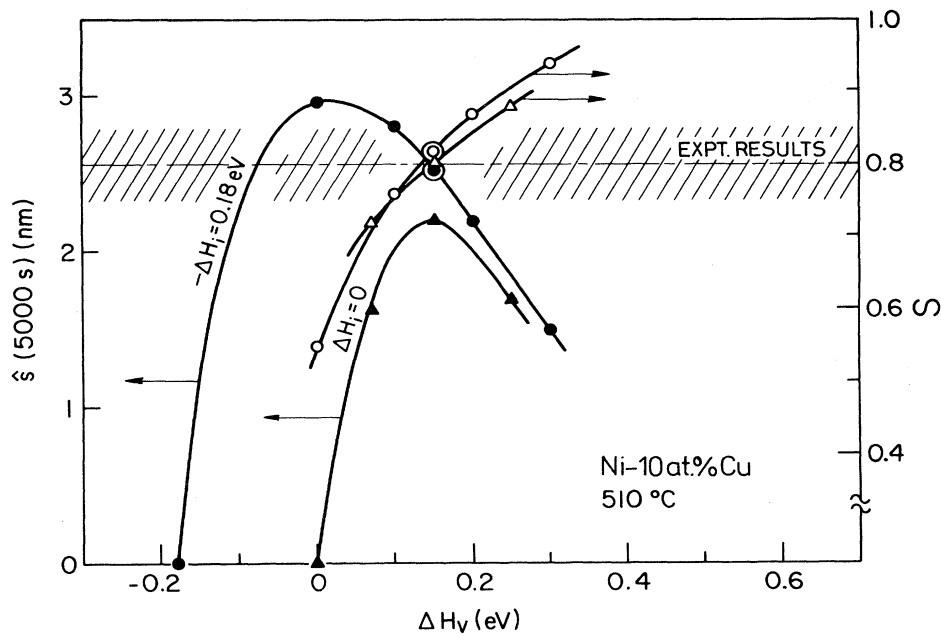


FIG. 9. Segregation dependence on ΔH_v (for constant $H_{Av}=1.00$ eV), for two different H_{Ai} , H_{Bi} , i.e., $H_{Ai}=0.30$ eV, $H_{Bi}=0.12$ eV, and $H_{Ai}=H_{Bi}=0.12$ eV. All else as for Fig. 8.

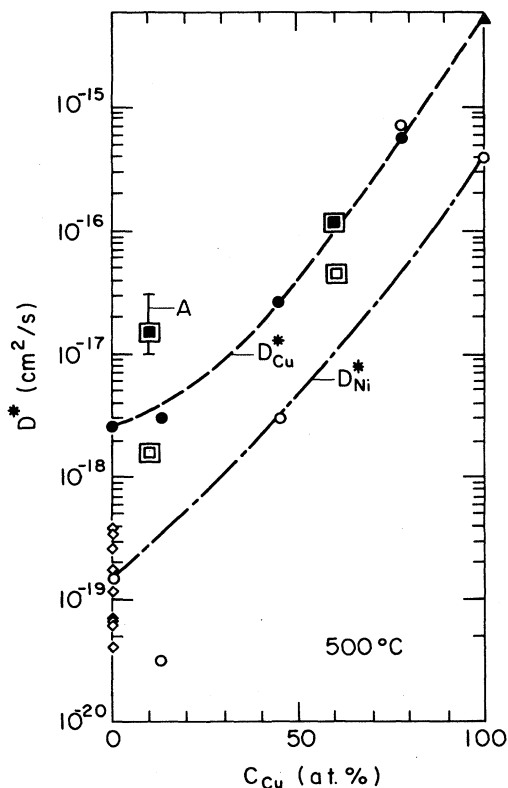


FIG. 10. Tracer diffusion data of Ni (open symbols: \diamond , \circ , \square) and Cu (filled symbols \blacktriangle , \bullet , \blacksquare) in the Ni-Cu system, obtained from the backdiffusion experiment, present paper (A), or calculated with the data given in Tables I and II (\blacksquare , \blacksquare), in comparison with literature data: Ref. 29 (\circ), Ref. 31 (\diamond), and Ref. 32 (\triangle). The broken lines serve as a guide for the eye.

tivity of the calculated values of \hat{s} and S to variations in H_{Ai} and H_{Bi} was also found for the Ni-60 at. % Cu alloy for $0.10 \leq H_{Ai} \leq 0.83$, and $0.04 \leq H_{Bi} \leq 0.77$ eV (for constant $\Delta H_i = -0.06$ eV). The reason why the calculations are more sensitive to changes in the vacancy parameters is because of our assumption (see Tables I and II) that the vacancies are significantly less mobile than the interstitial defects. Note that the steady-state profile of A atoms has been written in Eq. (21) as an image of the vacancy concentration profile. However, Eq. (21) can equally well be written using only the interstitial concentration profile. It is the additional assumption that one type of defect is less mobile which destroys the symmetry between vacancies and interstitials in the equations, and makes the calculations more sensitive to changes in the mobility of the slower defect.

Another result which occurs because of this assumed asymmetry can be found in Fig. 9. The rate at which the concentration gradients approach steady state for $\Delta H_v = 0$ and $\Delta H_i = -0.18$ eV (only interstitial contribution) differ markedly from the $\Delta H_v = 0.18$ eV and $\Delta H_i = 0$ (only vacancy contribution) case. That is, from Fig. 9 we see that S equals 0.55 for the only interstitial contribution case, but 0.84 for the only vacancy contribution case. The dominant cause for this result can be found in the response of the defect concentration profiles to changes in ΔH_v . Increasing ΔH_v reduces the net mobility of the slower moving defects (vacancies), and creates steeper vacancy concentration profiles in the near-surface region. Hence, \hat{s} (5000 s) decreases with increasing ΔH_v , because the depth of segregation is reduced. S increases to 0.84 for the only vacancy contribution case since \hat{s} (5000 s) is reduced substantially by increasing ΔH_v from 0 to 0.18 eV, but \hat{s} (1200 s) is relatively unchanged since insufficient time has elapsed for the effect of segregation at

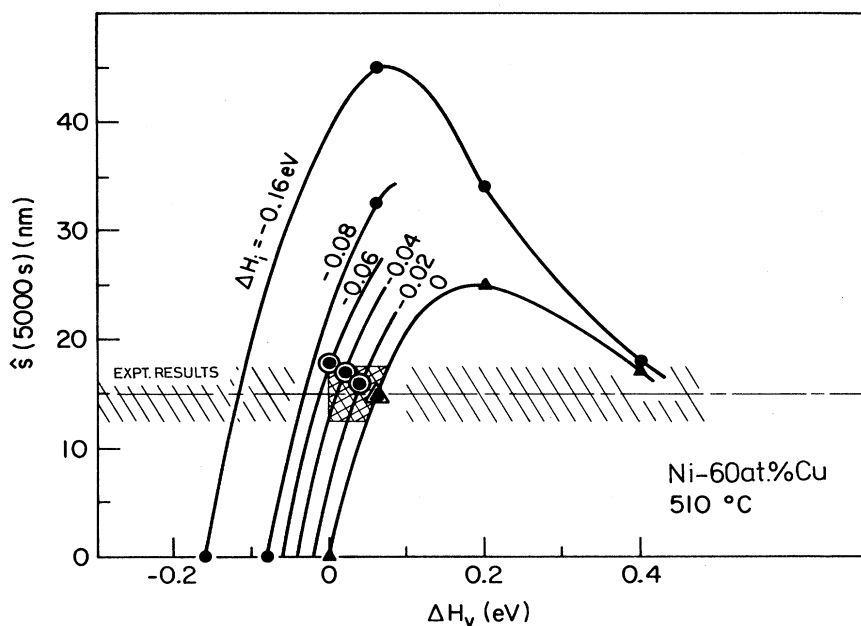


FIG. 11. Segregation dependence on ΔH_v (for constant $H_{Av} = 1.06$ eV) in Ni-60 at. % Cu, for different H_{Ai} , H_{Bi} , yielding different ΔH_i , with the condition $(H_{Ai} + H_{Bi})/2 = 0.20$ eV. All circled values fit the experimental results equally well. The cross-shaded region represents the possible range of parameter variations.

large depths to be significant.

Analogous to Fig. 9, \hat{s} as a function of ΔH_v is shown in Fig. 11 for the Ni-60 at. % Cu alloy, again for different values of ΔH_i ranging from -0.16 eV to zero. The upper limit of zero was chosen assuming that ΔH_i would not change sign in the alloy system; the same assumption seems reasonable for ΔH_v as well. According to the calculations shown in Fig. 11, there are two regions where the experimentally observed \hat{s} is reproduced, namely $0 \leq \Delta H_v \leq 0.06$ eV and $\Delta H_v \geq 0.4$ eV. The latter can be excluded by considering the surface concentrations of copper after 5000 s of irradiation, which in this alloy were found to be between 30 and 50 at. %. Such values are reproduced by the model calculations only for small ΔH_v , i.e., $\Delta H_v \leq 0.1$ eV, while for larger ΔH_v there is an increasing tendency to complete copper depletion at the surface.

The calculated depth profiles fit the experimental data for the 60-at. % Cu alloy equally well for both parameter sets given in Table II, i.e., for $\Delta H_v = 0.06$ eV and $\Delta H_i = 0$, or $\Delta H_v = 0$ and $\Delta H_i = -0.06$ eV, or for any combination as long as $|\Delta H_v| + |\Delta H_i| \sim 0.06$ eV. It appears from these results that differences in defect properties for the two alloy constituents are significantly less pronounced in the more concentrated 60-at. % Cu alloy than in the more dilute Ni-10 at. % Cu alloy.

VII. SUMMARY

A detailed and systematic experimental study of the temperature and dose dependences of RIS in two alloys, Ni-10 at. % Cu and Ni-60 at. % Cu, was performed. The results have been evaluated quantitatively using the concentrated alloy model developed by Wiedersich *et al.*⁶ Best-fit defect-solute parameters are listed in Tables I and II, and they agree well with the limited information available in the literature. In the 10-at. % Cu alloy, the model requires both preferential transport of nickel atoms toward the surface via the interstitial flux and preferential transport of copper atoms into the bulk via the vacancy flux to reproduce the measured concentration profiles. In the 60-at. % Cu alloy, the model explains the results equally well with preferential transport of nickel atoms by interstitials, preferential transport of copper atoms via vacancies, or by a combination of these two transport mechanisms.

ACKNOWLEDGMENTS

The authors are grateful to C. Abromeit and N. Q. Lam for providing the computer program for the calculations. We also thank P. Baldo, B. Kestel, and A. McCormick for their valuable assistance in the experiments. This work was supported in part by the U.S. Department of Energy.

- ¹Radiation Effects in Breeder Reactor Structural Materials, edited by M. L. Bleiberg and J. W. Bennett (The Metallurgical Society of AIME, New York, 1977).
- ²Workshop on Solute Segregation and Phase Stability During Irradiation, edited by J. O. Stiegler [J. Nucl. Mater. **83**, 1 (1979)].
- ³Comportement sous Irradiation des Matériaux Métalliques et des Composants des Coeurs des Réacteurs Rapides, edited by J. Poirier and J. M. Dupouy (Commissariat à l'Energie Atomique, Gif-Sur-Yvette, France, 1979).
- ⁴Irradiation Effects on Phase Stability, edited by J. R. Holland, L. K. Mansur, and D. I. Potter (The Metallurgical Society of AIME, New York, 1981).
- ⁵R. A. Johnson and N. Q. Lam, J. Nucl. Mater. **69 & 70**, 424 (1978).
- ⁶H. Wiedersich, P. R. Okamoto, and N. Q. Lam, J. Nucl. Mater. **83**, 98 (1979).
- ⁷G. Martin, Phys. Rev. B **21**, 2122 (1980).
- ⁸R. Cauvin and G. Martin, Phys. Rev. B **23**, 3322 (1981).
- ⁹L. E. Rehn, W. Wagner, and H. Wiedersich, Scr. Metall. **15**, 683 (1981).
- ¹⁰W. Wagner, V. Naundorf, L. E. Rehn, and H. Wiedersich, Surface Segregation in Concentrated Ni-Cu Alloys Under Irradiation, Effects of Radiation on Materials: Eleventh Conference, ASTM STP 782, edited by H. R. Brager and J. S. Perrin (American Society for Testing and Materials, Philadelphia, 1982), pp. 895-905.
- ¹¹R. Poerschke and H. Wollenberger, Thin Solid Films **25**, 167 (1975).
- ¹²R. Poerschke and H. Wollenberger, Radiat. Eff. **24**, 217 (1975); **49**, 225 (1980).
- ¹³W. Wagner, R. Poerschke, A. Axmann, and D. Schwahn, Phys. Rev. B **21**, 3087 (1980).
- ¹⁴W. Wagner, R. Poerschke, and H. Wollenberger, J. Phys. F **12**, 405 (1982).
- ¹⁵R. Sizmann, J. Nucl. Mater. **69 & 70**, 386 (1978).
- ¹⁶N. Q. Lam, S. J. Rothman, and R. Sizmann, Radiat. Eff. **23**, 53 (1974).
- ¹⁷A. Taylor, J. R. Wallace, D. I. Potter, D. G. Ryding, and B. Okray Hall, in Proceedings, International Conference on Radiation Effects and Tritium Technology for Fusion Reactors, Gatlinburg, Tennessee (Energy Research Development Agency, Springfield, Va., 1976), Vol. I, p. 158.
- ¹⁸D. K. Brice, Sandia Laboratories (Albuquerque, New Mexico) Report No. SLA-73-0416, (unpublished).
- ¹⁹K. Goto, T. Koshikawa, K. Ishikawa, and R. Shimizu, J. Vac. Sci. Technol. **15**, 1695 (1978).
- ²⁰L. I. Maissel, Handbook of Thin Film Technology, edited by L. I. Maissel and R. Glang (McGraw-Hill, New York, 1970), p. 440.
- ²¹T. Koshikawa, K. Goto, N. Sacki, R. Shimizu, and E. Sugata, Surf. Sci. **79**, 461 (1979).
- ²²A. C. Hindmarsh, Lawrence Livermore Laboratory Report UCID-30001 (unpublished).
- ²³W. B. Pearson, Handbook of Lattice Spacing and Structure of Metals and Alloys (Pergamon, New York, 1958).
- ²⁴V. K. Sethi and P. R. Okamoto, in Ref. 4, (1981) pp. 109-121.
- ²⁵C. A. English, B. L. Eyre, and J. Summers, Philos. Mag. **34**, 603 (1976).
- ²⁶T. M. Robinson, and M. L. Jenkins, Philos. Mag. A **43**, 999 (1981).
- ²⁷K. Schroeder, and E. Eberlein, Z. Phys. B **22**, 181 (1975).
- ²⁸R. Lennartz, F. Dworschak, and H. Wollenberger, J. Phys. F **7**, 2011 (1977).
- ²⁹K. Monma, H. Suto, and H. Oikawa, Nippon Kinzoku Gakkaishi **28**, 192 (1964).
- ³⁰W. Wycisk, Phd. thesis, Technische Universität Berlin, D83, 1977 (unpublished).
- ³¹M. Gründler and M. Feller-Kniepmeier, Z. Metallkd. **67**, 533 (1976), and references therein.
- ³²K. Maier, Phys. Status. Solidi A **44**, 567 (1977).
- ³³W. Schilling, G. Burger, K. Isebeck, and H. Wenzl, in Vacancies and Interstitials in Metals, edited by A. Seeger, D. Schumacher, W. Schilling, and J. Diehl (North-Holland, Amsterdam, 1970).